Morphology of critically sized crystalline nuclei at shear-induced crystal nucleation in amorphous solid

Bulat N. Galimzyanov, and Anatolii V. Mokshin

Citation: Journal of Rheology **62**, 265 (2018);
View online: https://doi.org/10.1122/1.5003238
View Table of Contents: http://sor.scitation.org/toc/jor/62/1
Published by the The Society of Rheology

Morphology of critically sized crystalline nuclei at shear-induced crystal nucleation in amorphous solid

Bulat N. Galimzyanov[a)] and Anatolii V. Mokshin

Department of Computational Physics, Institute of Physics, Kazan Federal University, 420008 Kazan, Russia

(Received 4 September 2017; final revision received 2 November 2017; published 1 December 2017)

Abstract

In this work, we study morphological characteristics of the critically sized crystalline nuclei at initial stage of the shear-induced crystallization of a model single-component amorphous (glassy) system. These characteristics are estimated quantitatively through statistical treatment of the nonequilibrium molecular dynamics simulation results for the system under steady shear at various (fixed) values of the shear rate $\dot{\gamma}$ and at different temperatures. It is found that the sheared glassy system is crystallized through nucleation mechanism. From the analysis of time-dependent trajectories of the largest crystalline nuclei, the critical size n_c and the nucleation time τ_c were defined. It is shown that the critically sized nuclei in the system are oriented within the shear-gradient xy-plane at moderate and high shear rates; and a tilt angle of the oriented nuclei depends on the shear rate. At extremely high shear rates and at shear deformation of the system more than 60%, the tilt angle of the nuclei tends to take the value $\simeq 45^\circ$ respective to the shear direction. We found that this feature depends weakly on the temperature. Asphericity of the nucleus shape increases with increasing shear rate that is verified by increasing value of the asphericity parameter and by the contour of the pair distribution function calculated for the particles of the critically sized nuclei. The critical size increases with increasing shear rate according to the power-law, $n_c \propto (\dot{\gamma}\tau_c)^{1/3}$, whereas the shape of the critically sized nucleus changes from spherical to the elongated ellipsoidal. We found that the n_c-dependencies of the nuclei deformation parameter evaluated for the system at different temperatures and shear rates are collapsed into unified master-curve. https://doi.org/10.1122/1.5003238

I. INTRODUCTION

Due to a disordered structure, the amorphous materials (metallic glasses, polymeric, and colloidal amorphous solids) have unique mechanical and physical properties, which allow one to find their practical applications in photonics, medicine, and electronics [1–7]. Furthermore, the microscopic structure of disordered systems under different mechanical deformations (compression, shear, etc.) is of a special interest [8]. In particular, understanding of physical mechanisms of the steady shear influence on the microscopic structure of the systems could provide a possibility to develop practical tools to control the structural ordering process [2,7,9–14].

A large number of experimental and simulation studies provide indications that the steady shear applied to metastable disordered systems (supercooled liquids and amorphous solids) generates a microscopic structure anisotropy in these systems [7,13–22]. It is clear that the anisotropy arisen in the disordered systems under shear leads to change of morphological characteristics of emerging crystalline structures. Therefore, the mechanical and rheological properties of the systems can be significantly dependent on the anisotropy. This is confirmed by results of a large number of studies [1,7,14,23–32]. So, for example, Kumaraswamy and coworkers [22] have revealed experimentally that nonspherical ordered structures oriented along the shear direction occur for the case of polydisperse isotactic polypropylene melt under intensive shear. Moreover, they found that these structures appear as precursors of crystallization at a temperature below the melting point; and morphological properties of these precursors have a significant impact on the overall crystallization kinetics. On the basis of experimental and simulation studies done by Petekidis and co-workers [21,32,33], it was found that the microscopic structure of polymeric colloidal glasses under shear changes with increasing shear rate. This is directly manifested in the shape of the evaluated density distribution $g(x, y)$. Namely, the function $g(x, y)$ characterizing the particles distribution within the shear-gradient plane starts to change its shape under applied shear flow. Then, it is reasonably to expect that the observed structural changes of the systems may do impact on their rheological properties. It was found in [33] that the ordered structures forming under shear are not stable thermodynamically, and they may be characterized by the rheological aging. These results are supplemented by simulation studies. For example, simulation results of Blaak *et al.* have revealed that the elongated crystalline nuclei oriented along the shear direction occur at shear-induced crystallization of colloidal suspensions [16]. Here, a tilt angle of the nucleus increases with increasing shear rate. On the other hand, Graham and Olmsted found that nonspherical elongated nuclei occur in sheared polymer melts, and such shape has been mentioned as shish-kebab [26]. According to the results of [26], the crystal nucleation may be accelerated by shear. Note, the similar results were also obtained for the case of crystallization of model glassy systems at homogeneous shear [7,15,34]. It was found in [7,15,34] that steady

[a)]Author to whom correspondence should be addressed; electronic mail: bulatgnmail@gmail.com

shear can both accelerate and suppress the crystal nucleation process in the glassy systems.

In spite of a large number of studies mentioned above, there are still a lot of unclear points related with the influence of a steady homogeneous shear on the morphology of crystalline structures emerging in amorphous solids [15,18,35,36]. For example, the physical mechanisms determining the crystalline nuclei asphericity at the initial stage of crystallization, when the size of these nuclei is comparable with a critical size, are debated [7,15,16,26]. According to the classical nucleation theory [37–39], only the critically sized nuclei may demonstrate a stable growth. Moreover, from the experimental point of view, it is not so easy to evaluate such morphological characteristics as the critical size and the shape of the crystalline nuclei in the atomistic and molecular systems under shear with different rates [13,33,40]. This is especially appropriate for the case of deep supercooling levels, when the temperatures are below the glass transition temperature T_g.

In the present work, we study the microscopic mechanisms of shear-induced crystallization of a single-component glassy system at different temperatures. The main attention is paid to study morphological characteristics of the critically sized crystalline nuclei in the system under a homogeneous shear with various (fixed) shear rates. These characteristics are considered as the terms dependent on the critical deformation $\gamma_c \equiv \dot{\gamma}\tau_c$. Here, the dimensionless quantity γ_c is the deformation of the system under shear with the rate $\dot{\gamma}$ at the time moment $\tau_c \equiv \tau(n_c)$, i.e., when the critically sized n_c nucleus appears. In other words, the quantity γ_c corresponds directly to the time scale of the nucleation time τ_c. We find that the homogeneous shear initiates the structural ordering in the glassy system through the crystal nucleation mechanism, where the nuclei with pronounced asphericity of their shape and oriented along the shear direction are formed. Simulation details and cluster analysis are presented in Sec. II. The results are given and discussed in Sec. III. Finally, the main results will be summarized in the conclusion.

II. SIMULATION DETAILS AND CLUSTER ANALYSIS

Molecular dynamics simulations are performed for the single-component system, where the interaction between the particles is defined through the short-ranged oscillatory Dzugutov potential (Dz-system) [41,42]. The specific shape of the potential allows one to reproduce effectively the effect of electron screening for the ion-ion interaction in metals. In addition, the system with such potential is capable to generate a stable amorphous state [7,34,43].

To realize the homogeneous shear, the SLLOD-algorithm is applied [12], where the shear velocity

$$\vec{u}_i = \dot{\gamma} y_i \vec{e}_x \tag{1}$$

is added to the x-component of intrinsic (thermal) velocity $\vec{v}_i$ of each particle of the system. As a result, equations of motion are [12]

$$\frac{d\vec{r}_i}{dt} = \vec{v}_i + \dot{\gamma} y_i \vec{e}_x + \zeta \vec{r}_i, \tag{2a}$$

$$\frac{d\vec{v}_i}{dt} = \frac{\vec{F}_i}{m} - \dot{\gamma} v_{yi} \vec{e}_x - (\varrho + \zeta)\vec{v}_i. \tag{2b}$$

Here, $\vec{r}_i(x_i, y_i, z_i)$ and $\vec{v}_i(v_{xi}, v_{yi}, v_{zi})$ are the position and velocity of the ith particle, respectively ($i = 1, 2, \ldots N$, where N is the number of particles); ϱ and ζ are the parameters of thermostat and barostat, respectively. In the present work, the homogeneous shear is applied with different fixed shear rates: $\dot{\gamma} = 0.0001$, 0.0005, 0.001, 0.002, 0.005, 0.008, and $0.01\,\tau^{-1}$. Realization of the homogeneous shear is schematically presented in Fig. 1.

The considered three-dimensional system consists of $N = 6912$ identical particles located within the cubic simulation cell. The Lees–Edwards periodic boundary conditions are applied in both the gradient y- and vorticity z-directions [44]. The ordinary periodic boundary conditions are also applied in the shear x-direction. The instantaneous velocities and trajectories of the particles are determined by integration of the equations of motion (2) using the Verlet algorithm with the time step $\Delta t = 0.005\,\tau$. All simulations are performed in the isobaric-isothermal ensemble, where the temperature T and the pressure p are controlled by the Nose-Hoover thermostat and barostat, respectively. In the present work, the standard Lennard-Jones units are used: σ is the effective particle diameter; ϵ is the energy unit; $\tau = \sigma\sqrt{m/\epsilon}$ is the time unit, where m is the mass of the particle; the temperature T in units of ϵ/k_B, where k_B is the Boltzmann constant; the pressure p in units of ϵ/σ^3; the shear rate $\dot{\gamma}$ in units of τ^{-1}.

Molecular dynamics simulations are realized as follows: At first, a liquid sample is equilibrated at the temperature $T = 2.3\,\epsilon/k_B$ and at the pressure $p = 14\,\epsilon/\sigma^3$, that is above the melting temperature of the system $T_m \simeq 1.51\,\epsilon/k_B$ at

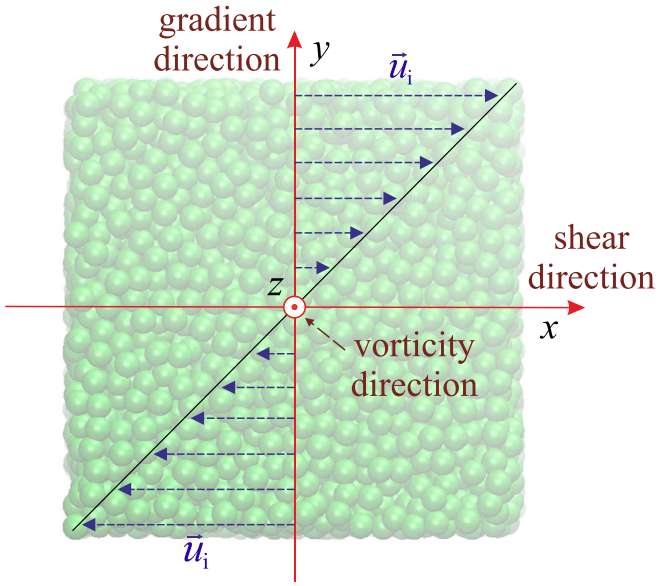

FIG. 1. Schematic representation of the homogeneous shear realization with a linear velocity profile: Green spheres show the particles of a system; the blue arrows characterize the shear directions with rate $\vec{u}_i$ ($i = 1, 2, \ldots, N$). The axis OX is associated with the shear-direction; the axis OY corresponds to the gradient-direction; the axis OZ indicates the vorticity-direction.

considered pressure (the phase diagram of the Dz-system can be found in [42]). Second, the glassy samples are prepared through rapid cooling of the equilibrated liquid with the cooling rate of $0.001\,\epsilon/(k_B\tau)$ to the temperatures $T=0.05$, 0.15, and $0.5\,\epsilon/k_B$, that is much lower than the glass transition temperature $T_g \simeq 0.65\,\epsilon/k_B$ of the system. Thus, one hundred independent glassy samples are prepared for each considered (p, T) thermodynamic state, that are required to perform a statistical treatment of the simulation results. And, finally, each glassy sample is exposed to a homogeneous shear on the time scale ~100 000 simulation steps.

To detect the crystalline structures, the cluster analysis based on the estimation of the bond orientational order parameters was applied [45,46]. Namely, following to Steinhardt *et al*. [45], the local orientational order parameters are defined as

$$q_l(i) = \left(\frac{4\pi}{2l+1} \sum_{m=-l}^{l} \left| \frac{1}{n_b^{(i)}} \sum_{j=1}^{n_b^{(i)}} Y_{lm}\left(\theta_{ij}, \varphi_{ij}\right) \right|^2 \right)^{1/2}, \quad (3)$$

where

$$l = 4,\ 6,\ 8.$$

Also we estimate the value of the global orientational order parameter as an average of $q_6(i)$ (i.e., at $l=6$) over all the particles of the system [45]

$$Q_6 = \left(\frac{4\pi}{13} \sum_{m=-6}^{6} \left| \frac{\sum_{i=1}^{N} \sum_{j=1}^{n_b^{(i)}} Y_{6m}\left(\theta_{ij}, \varphi_{ij}\right)}{\sum_{i=1}^{N} n_b^{(i)}} \right|^2 \right)^{1/2}. \quad (4)$$

Here, $n_b^{(i)}$ is the number of neighbors of the ith particle; $Y_{lm}(\theta_{ij}, \varphi_{ij})$ are the spherical harmonics; θ_{ij} and φ_{ij} are the polar and azimuthal angles, respectively. As a rule, even spherical harmonics with the indexes $l=4$, 6, and 8 are sufficient to recognize the presence of the ordered domains in the system. For example, the local orientational order parameters q_4, q_6, q_8 take nonzero values for the particles forming *sc* (simple cubic), *icos* (icosahedral), *bcc* (base-centered cubic), *fcc* (face-centered cubic), and *hcp* (hexagonal close-packed) crystalline structures [47]. For a disordered glassy system, the local orientational order parameters obey a normal distribution, whereas the value of the parameter Q_6 tends to zero for this case [45,48]. The order parameters q_i and Q_j, where $i, j = 4, 6, 8, \ldots$, take unique values for specific crystalline structures that allows one to identify these structures in the considered system [45]. In particular, according to the original normalization of the parameter Q_6, the parameter Q_6 is 0.575 for the perfect *fcc* lattice; one has $Q_6 = 0.485$ for the perfect *hcp* lattice and $Q_6 = 0.663$ for the *icosahedral* lattice. The smaller values can be due to the presence of defects.

One of the key conditions, by which the particle is identified as entering into an ordered phase, is so-called coherence condition [48]

$$\left| \sum_{m=-6}^{6} \vec{q}^{\,*}_{6m}(i) \cdot \vec{q}_{6m}(j) \right| \geq 0.5, \quad (5a)$$

$$\vec{q}_{6m}(i) = \frac{q_{6m}(i)}{\sqrt{\sum_{m=-6}^{6} |q_{6m}(i)|^2}}. \quad (5b)$$

Namely, according to the scheme suggested in [48], the pair of particles i and j are considered as "solidlike" if the dot-product $\vec{q}^{\,*}_6(i) \cdot \vec{q}_6(j)$ exceeds the threshold value 0.5. In this case, the nearest neighborhood of the ith particle must contain seven and more solidlike particles, for which condition (5) is satisfied.

For quantitative characterization of the crystalline nuclei shape, we evaluate the asphericity parameter [46]

$$S_0 = \left\langle \frac{(I_{xx}-I_{yy})^2 + (I_{xx}-I_{zz})^2 + (I_{yy}-I_{zz})^2}{2(I_{xx}+I_{yy}+I_{zz})^2} \right\rangle, \quad (6)$$

where

$$I_{\alpha\beta} = m \sum_{i=1}^{n_c} (\vec{r}_i^{\,2}\delta_{\alpha\beta} - \vec{r}_{i\alpha}\vec{r}_{i\beta}) \quad (7)$$

are the moments of inertia ($\alpha\beta \in \{x, y, z\}$). Here, $|\vec{r}_i|$ is the distance between the nucleus center-of-mass and the position of ith solidlike particle; $\delta_{\alpha\beta}$ is the Kronecker delta. Thus, for the case of a perfect spherical shape, we have $S_0 = 0$; the parameter is $S_0 \to 1$ for extremely elongated shape.

By means of the cluster analysis, we obtain for each αth simulation run the growth trajectories of the largest crystalline nucleus, $n_\alpha(t)$. Here, the quantity $n_\alpha(t)$ indicates that the nucleus of the size n appears at the time t during the αth simulation run, where $\alpha = 1, 2, \ldots, 100$. These trajectories extracted from the different simulation runs are treated within the mean-first-passage-time method [36,49]. According to this method, the curve $\tau(n)$ is defined, which is known as the mean-first-passage-time curve and which characterizes the average time of the first appearance of the largest nucleus with given size n (for details, see [36,49]). The critical size n_c and the average nucleation (or waiting) time for the nucleus τ_c, are defined from the analysis of the curve $\tau(n)$ and of the first derivative $\partial\tau(n)/\partial n$, according to the scheme suggested in [36]. In the case of activation type processes, the curve $\tau(n)$ characterizes by three regimes: (i) the first regime is associated with prenucleation, where the small values of n correspond to $\tau(n)$ with zero value; (ii) the second regime, in which the curve $\tau(n)$ has the pronounced nonzero slope, contains information about a nucleation event. Namely, detected from the first derivative $\partial\tau(n)/\partial n$ location of an inflection point in the curve $\tau(n)$ for this regime defines the critical size n_c, whereas $\tau(n_c) \equiv \tau_c$ is directly associated with the nucleation time of the critically sized nucleus; (iii) the third regime, where the slope of $\tau(n)$ decreases corresponds to growth of the nucleus. Note that in the present work we focus on the characteristics for the largest crystalline nucleus.

III. RESULTS

A. Crystalline structures

Information about structural transformations in the glassy system at homogeneous shear is obtained through evaluation

of the orientational order parameters q_4, q_6, q_8, and Q_6. The most probable values of the order parameters have been computed by averaging the data obtained from one hundred independent numerical experiments at different shear rates $\dot{\gamma}$. As an example, Fig. 2(a) shows the time-dependent order parameter Q_6 computed for the system at the temperature $T = 0.15\,\epsilon/k_B$ and at the shear rate of $\dot{\gamma} = 0.001\,\tau^{-1}$. Initially, the order parameter Q_6 takes the small value ~0.023, which corresponds to a disordered system. Further, the glassy system is crystallized after initiation of the shear deformation. Namely, the parameter Q_6 begins to increase after lag time $\sim 70\,\tau$ and at $t > 250\,\tau$ the parameter goes to saturation with value $Q_6 \simeq 0.47$, which corresponds to a completely ordered system. The sigmoidal shape of the $Q_6(t)$-curve is typical for the activation processes when, for example, the crystallization occurs through the nucleation mechanism [15,50]. A similar scenario of structural ordering is also observed at other shear rates and temperatures with a difference only in the crystallization time scales.

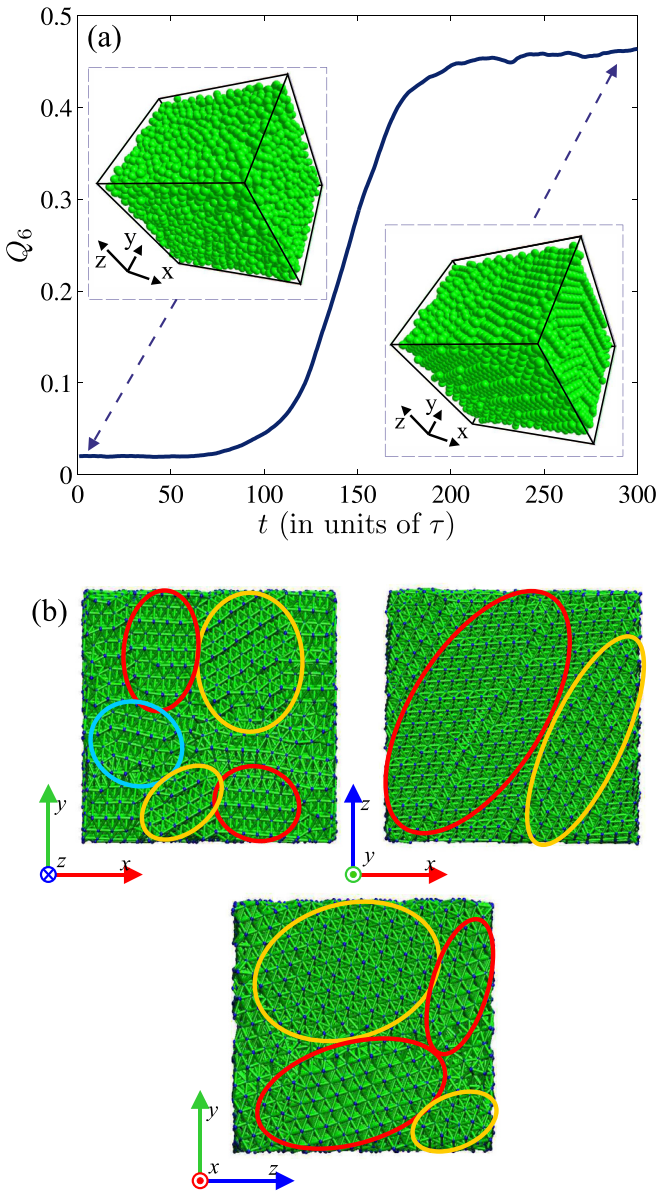

FIG. 2. (a) Time-dependent orientational order parameter $Q_6(t)$ evaluated for the system at the temperature $T = 0.15\,\epsilon/k_B$ and at shear rate $\dot{\gamma} = 0.001\,\tau^{-1}$. Insets: Instantaneous configurations of a system corresponding to values $Q_6 \simeq 0.023$ (left inset) and $Q_6 \simeq 0.47$ (right inset). (b) Snapshots of the simulation cell corresponding to the system at the temperature $T = 0.15\,\epsilon/k_B$ and the shear rate $\dot{\gamma} = 0.001\,\tau^{-1}$, when an ordered state is achieved. Here, the order parameter Q_6 is ~0.47. In fact, the system represents a nanocrystalline solid consisted of an assembly of crystallites with disordered orientations, and the degree of order achieved by the system is low in comparison to that of a perfect crystal.

Characteristic directions of the crystalline lattice were initially estimated for the critically sized nucleus. As we found, there is no alignment of the crystal structure of the nuclei along the shear- and/or gradient-directions. Moreover, the correspondence between orientation of the crystal planes and the specific shear directions was also not detected even for the completely ordered systems, where the order parameter Q_6 takes its largest value. This is seen from snapshots of the system at $T = 0.15\,\epsilon/k_B$ and shear rate $0.001\,\tau^{-1}$ [see Fig. 2(b)].

Figure 3 shows the distributions $P(q_4)$, $P(q_6)$, and $P(q_8)$ for the system at the temperature $T = 0.15\,\epsilon/k_B$ and at the shear rate $\dot{\gamma} = 0.001\,\tau^{-1}$, when the system is completely crystallized (i.e., when the system corresponds to the state with $Q_6 \simeq 0.47$). The normal distributions $P(q_4)$, $P(q_6)$, and $P(q_8)$ corresponded to the glassy system before initiation of the homogeneous shear are also presented in Fig. 3 (here, the order parameter is $Q_6 \simeq 0.023$). After initiation of the shear, the structural ordering degree increases. This is also manifested by a change of shapes of $P(q_4)$, $P(q_6)$, $P(q_8)$ and by appearance of peaks located at high values of the parameters q_4, q_6, and q_8. The locations of these peaks in the distributions $P(q_4)$, $P(q_6)$, and $P(q_8)$ correspond to structures with the *fcc* and *hcp*-symmetries. The fraction of "*fcc*-particles" is ~60%–70%, whereas the fraction of "*hcp*-particles" is ~30%–40%. Moreover, locations of the peaks in the distributions $P(q_4)$, $P(q_6)$, and $P(q_8)$ corresponding to $q_4 \simeq 0.21$, $q_6 \simeq 0.57$, and $q_8 \simeq 0.41$ indicate the *fcc*-symmetry. The peaks in the distributions at $q_4 \simeq 0.11$, $q_6 \simeq 0.48$, and $q_8 \simeq 0.31$ correspond to the particles forming the *hcp* lattice [47]. In accordance with the equilibrium phase diagram of the Dzugutov system, the temperature region along the isobar

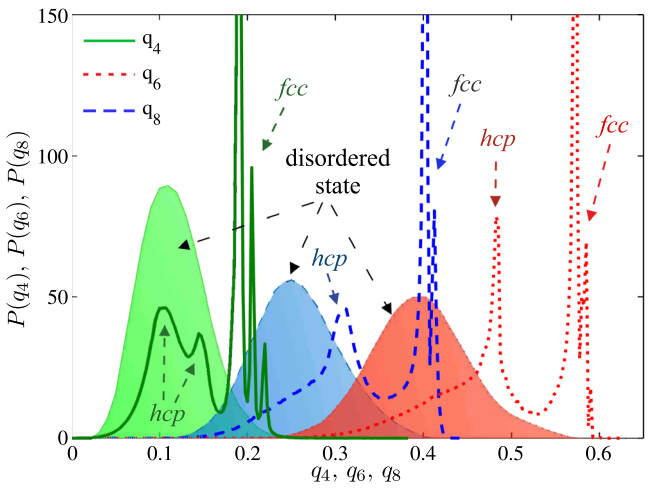

FIG. 3. Distributions $P(q_4)$, $P(q_6)$, and $P(q_8)$ evaluated for the Dz-system at the temperature $T = 0.15\,\epsilon/k_B$ with $Q_6 \simeq 0.47$ crystallized at the shear rate $\dot{\gamma} = 0.001\,\tau^{-1}$.

$p = 14\,\epsilon/\sigma^3$ includes the crystalline phases with the *fcc* and *hcp* lattices [41,42]. In particular, at deformation of an amorphous system by shock waves, it was observed in [42,51] a phase transition into the high-pressure states with *fcc* or *hcp* crystalline phase. Both lattice types appear simultaneously and have a slight difference due to defects in the crystalline structure caused by the shock waves.

B. Critically sized crystalline nuclei under shear

Results of the cluster analysis reveal that the structural ordering in the glassy Dz-system occurs through the formation of small-sized crystalline nuclei consisting mainly of 30–50 particles. By the mean-first-passage-time method, the critical size n_c and the nucleation time τ_c have been evaluated for the system at different temperatures and shear rates [15,49]. Figure 4(a) shows the nucleation time τ_c as a function of the critical deformation γ_c evaluated at different temperatures. We found different regimes in γ_c-dependencies of τ_c. Namely, the nucleation time decreases at small and moderate shear rates and it increases at high shear rates. The nucleation time decreases from $\tau_c \simeq 125 \pm 15\,\tau$ to $\tau_c \simeq 40 \pm 6\,\tau$ with an increasing shear rate from $\dot{\gamma} = 0.0001\,\tau^{-1}$ ($\gamma_c \simeq 0.0125$) to $\dot{\gamma} = 0.002\,\tau^{-1}$ ($\gamma_c \simeq 0.08$). The nucleation time increases from $\tau_c \simeq 41 \pm 5\,\tau$ to $\tau_c \simeq 53 \pm 10\,\tau$ at increasing shear rate from $\dot{\gamma} = 0.005\,\tau^{-1}$ ($\gamma_c \simeq 0.205$) to $\dot{\gamma} = 0.01\,\tau^{-1}$ ($\gamma_c \simeq 0.53$) in the considered temperature range $T \in [0.05;\ 0.5]\,\epsilon/k_B$. Such a nonmonotonic γ_c-dependence of the nucleation time τ_c is due to the antagonistic impact of shear flow on the nucleation process. This effect was also discussed in [7,15]. As discussed in [15], such a nonmonotonic behavior of τ_c is due to the impact of shear deformation on the kinetic and thermodynamic aspects of the crystal nucleation in this system. Namely, a slow shear-flow accelerates the nucleation through the attachment rate, whereas the high shear rates destabilize the critical nuclei and reduce the probability of the particle attachment. On the other hand, a shear flow gives rise to "pressure anisotropy" [52] manifested in the fact that the diagonal components of the pressure tensor begin to differ. This effect leads to anisotropy of the interfacial free energy. Moreover, the shear deformation introduces an elastic energy into the system and, thereby, it has an impact on the thermodynamic characteristics of crystal nucleation (the nucleation barrier, the interfacial free energy, etc.) [19,53].

Although there are known experimental data characterizing the crystal nucleation in amorphous systems under shear, a comparison of different experimental data and results of the numerical simulation is a nontrivial task. In fact, these systems are characterized by various physical, chemical, and rheological properties, and the systems are studied at different thermodynamic and deformation conditions. Nevertheless, there are common regularities in structural ordering in these systems. Namely, the slow shear deformations accelerate the ordering, whereas the large shear rates suppress the crystallization. As a result, the strain-dependencies of the crystallization (nucleation) time must be characterized by a minimum. Therefore, it is reasonable to propose that such dependencies can be represented in the unified scaled form

$$\frac{\tau_c}{\tau_m} = f\left[\left(\frac{\gamma_c}{\gamma_m}\right)^{\xi}\right]. \tag{8}$$

Here, $f[\ldots]$ is a universal function and τ_m is the location of the minimum in the dependence $\tau_c(\gamma_c)$, whereas γ_m is the value of the critical deformation γ_c at the time τ_m. Further, the dimensionless positive parameter ξ can be considered as the characteristic of glass-forming ability of the system [36,54,55].

In Fig. 4(b), the scaled time τ_c/τ_m is presented as a function of the scaled critical deformation $(\gamma_c/\gamma_m)^{\xi}$ for different systems under shear: our simulation results for the Dzugutov system (Dz); experimental data for colloidal system (CS) [56], and two polymer systems (PS) [57] and (sP) [58]. For the case of CS and PS systems, the data for the induction time τ_{ind} vs the critical deformation γ_c were taken. As shown in Fig. 4(b), all the data collapse onto unified curve. This is evidence that the scaling relation (8) is valid. Here, the parameter ξ takes the next values: $\xi = 0.935$ for the Dzugutov system, 1.282 for the CS-system, 2.33 for the PS-

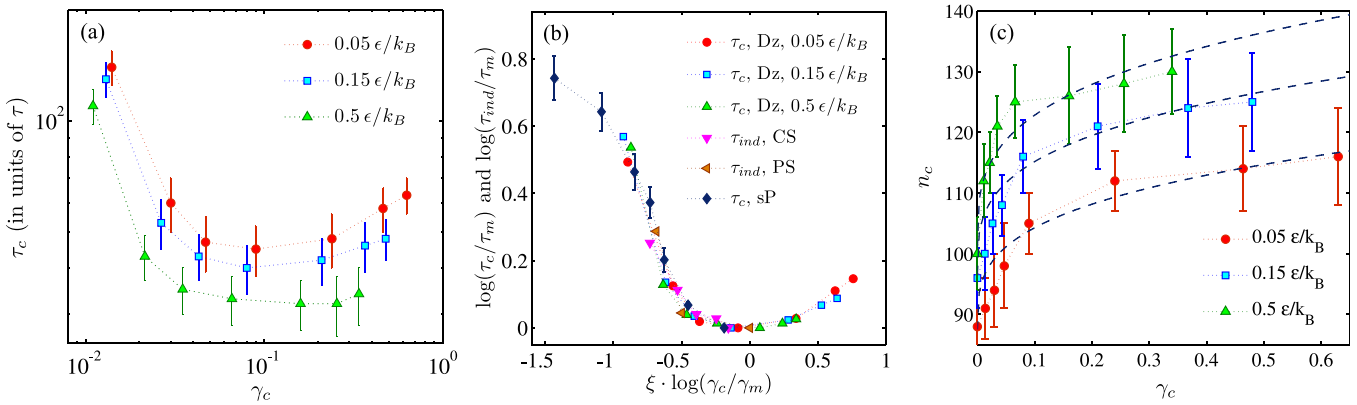

FIG. 4. (a) Nucleation time τ_c as a function of critical deformation γ_c evaluated for Dz-system at different temperatures. (b) Scaled nucleation time τ_c/τ_m and induction time τ_{ind}/τ_m as a function of scaled critical deformation $(\gamma_c/\gamma_m)^{\xi}$. Here, τ_m and γ_m are the parameters defined the minimum of the dependence $\tau_c(\gamma_c)$ [and $\tau_{ind}(\gamma_c)$]. Symbols (○), (□), and (△) indicate simulation results for the Dzugutov system at different temperatures, whereas symbols (▽), (◁), and (◇) correspond to experimental data for colloidal system (CS) [56] and for two polymer systems: (PS) [57] and (sP) [58]. (c) Critical size n_c vs γ_c. Dashed curves are results of fit in Eq. (15).

system, and 1.89 for the sP-system. Thus, the parameter takes the lowest value for the atomistic single-component Dzugutov system, and it takes the larger values for the polymer and colloidal systems with better glass-forming ability properties.

It should be noted that the crystal nucleation in amorphous solid (glass) differs from crystal nucleation in supercooled liquid. At low and moderate levels of supercooling corresponding to a liquid (supercooled) phase, the nucleation rate is determined mainly by the thermodynamic factor [15,36,37]. For a glassy phase with deep levels of supercooling, the nucleation is driven by the kinetic features of the system. Competition between the thermodynamic and kinetic aspects is clearly manifested in appearance of the characteristic maximum in the temperature dependence of the nucleation rate [37–39]. Influence of the shear on crystallization of the supercooled liquid and glass is also different. In particular, for the case of a liquid, the shear deformation increases the viscosity and, thereby, nucleation is suppressed [19,59]. For a glassy system, the shear increases *effectively* the mobility of particles and, thereby, the shear decreases the viscosity.

The system evolves at temperatures much below the glass transition temperature T_g. And, therefore, detection of the nucleation event for the system at zeroth shear may seem surprising. Actually, features of the microscopic kinetics of a glass change with moving over phase diagram for the range of high pressures. Namely, at high pressures the structural relaxation as well as the transition of the glassy system into a state with the lower free energy proceeds over shorter time scales [60]. As we found, the nucleation event is detectable within the simulation time scales for the Dz-system at the thermodynamic states with pressures $p \geq 12\,\epsilon/\sigma^3$ [36].

In Fig. 4(c), the quantity n_c as a function of the critical deformation γ_c evaluated at different temperatures is presented. In the absence of shear, for the considered temperature range $T \in [0.05;\, 0.5]\,\epsilon/k_B$, the critical size increases with temperature by several tens of particles. This is in agreement with classical nucleation theory [37,38], according to which $n_c = (32\pi\gamma_\infty^3)/(3\rho_c|\Delta\mu|^3)$. Here, γ_∞ is the interfacial free energy, $|\Delta\mu|$ is the difference of the chemical potential per phase unite in the melt (glass) and the crystal. Then, taking into account that the chemical potential difference $|\Delta\mu|$ is proportional the supercooling, $\Delta T = T_m - T$

$$|\Delta\mu| \sim \frac{\Delta T}{T_m},$$

one has that the critical size n_c increases with increasing temperature. Further, with increase of shear rate within the range $\dot\gamma \in [0.0001;\, 0.01]\,\tau^{-1}$, the critical size increases from $n_c \simeq 88$ to $n_c \simeq 130$ particles. As shown in Fig. 4(c), at the low shear rates $\dot\gamma < 0.001\,\tau^{-1}$, the nuclei appear at critical deformation $\gamma_c = 0.02$, whereas at high shear rates the formation of the nuclei occurs at the larger deformations. Namely, at the shear rate $\dot\gamma = 0.01\,\tau^{-1}$, the nuclei appear at the critical deformation $\gamma_c > 0.3$. The large values of γ_c are due to the high shear rates inhibit the crystal nucleation, which was previously discussed in [15,19].

For the crystalline nuclei with sizes ≤ 100 particles, it is quite reasonable within the statistical treatment to characterize their shape as the quantity averaged over data of independent experiments. This averaging procedure is denoted by $\langle\ldots\rangle$ in Eq. (6). As shown from Fig. 5(a), for a shear-free system as well as for the system at small shear rates $\dot\gamma < 0.001\,\tau^{-1}$, the asphericity parameter takes the values $S_0 < 0.02$. It indicates that the critically sized nucleus approximate a symmetric shape close to be a spherical. Further, the quantity S_0 increases from $\simeq 0.005$ to $S_0 \simeq 0.045$ with the increasing critical deformation γ_c that is due to the increase of the nucleus shape asphericity. Homogeneous steady-state shear promotes local rearrangements of the particles and leads effectively to an increase of particle mobility. Therefore, the system temperature takes a

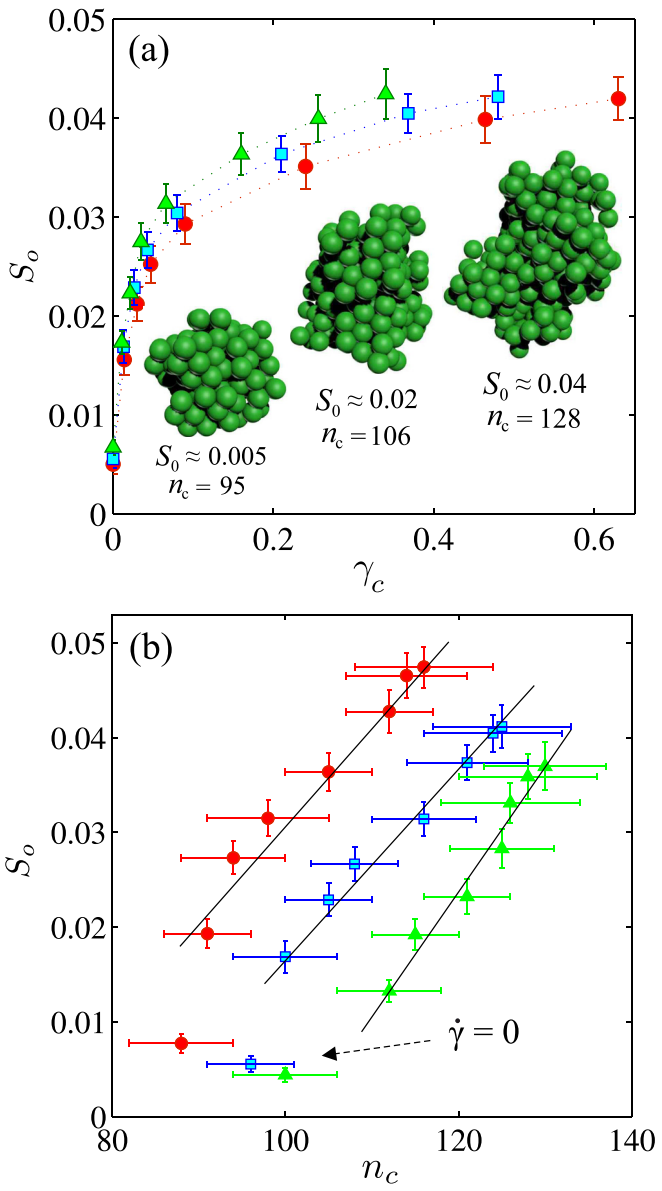

FIG. 5. (a) Asphericity parameter S_0 as a function of the critical deformation γ_c. Insets show the critically sized nuclei with various sizes and shapes. (b) Correlation between the asphericity parameter S_0 and the critical size n_c at different temperature of the system. Here, circles correspond to the system at $T = 0.05\,\epsilon/k_B$, squares correspond to $T = 0.15\,\epsilon/k_B$, and triangles correspond to $T = 0.5\,\epsilon/k_B$.

sense of the effective parameter [61], which increases with increase of the shear rate (Fig. 4 in [15]). Moreover, there is anisotropy of interfacial free energy due to shear. Then, the system with a specific characteristic interparticle interaction must be characterized by a limit value of curvature of the solid (crystal)-liquid interface; while the geometries with larger values of curvature will be unstable. As a result, a plateau in the γ_c-dependence of the asphericity parameter appears and saturation of the γ_c-dependence of the critical size is observed at high shear rates. Therefore, it is remarkable that the γ_c-dependence of S_0 is correlated with such a dependence of n_c. One can see from Fig. 5(b) that both quantities S_0 and n_c are correlated, and a larger value of the asphericity parameter S_0 correspond to a larger value of the critical size n_c. This scenario differs from crystal nucleation without external mechanical drive, where $S_0 \propto 1/n_c$ [46].

Projections of the pair-distribution function $g(r)$ onto the shear-gradient xy and the shear-vorticity xz planes were defined for particles of the critically sized nucleus as the next

$$g_c(x,y) = \left\langle \frac{1}{n_c} \sum_{i=1}^{n_c} \sum_{j>i}^{n_c} \delta\left(\vec{r} - \vec{r}_{ij}(x,y)\right) \right\rangle \tag{9}$$

and

$$g_c(x,z) = \left\langle \frac{1}{n_c} \sum_{i=1}^{n_c} \sum_{j>i}^{n_c} \delta\left(\vec{r} - \vec{r}_{ij}(x,z)\right) \right\rangle. \tag{10}$$

Here, $\langle \ldots \rangle$ means an averaging over data of independent simulation runs. At evaluation of the distributions $g_c(x,y)$ and $g_c(x,z)$, the positions of particles were determined with respect to the geometric center of a nucleus.

The distributions $g_c(x,y)$ for the system at the temperature $T = 0.15\,\epsilon/k_B$ and at the shear rates $\dot{\gamma} = 0$, 0.0005, 0.005, and $0.01\,\tau^{-1}$ are shown in Fig. 6. Further, Fig. 7 presents the distributions $g_c(x,z)$ for the shear-free system at the temperature $T = 0.15\,\epsilon/k_B$ and for the system at the shear rate $0.01\,\tau^{-1}$. As shown, the closed lines corresponding to the first, second, and third coordinations are well recognizable in these distributions. At the absence of a shear, the contours of the distributions $g_c(x,y)$ and $g_c(x,z)$ are circular, that is evidence of a spherical shape of the nucleus. As can be seen from contours of $g_c(x,y)$ and $g_c(x,z)$, the nucleus asphericity becomes more pronounced with shear increase [Figs. 6(b)–6(d), and Fig. 7(b)]. This is also observed at other considered temperatures, not presented in Figs. 6 and 7.

The contours of the distributions $g_c(x,y)$ and $g_c(x,z)$ change from circular to elliptical at increasing shear rate $\dot{\gamma}$. The long axis of the elliptic contour of $g_c(x,y)$ is oriented with respect to the gradient direction [see Figs. 6(b)–6(d)]. At the same time, the orientation of this ellipse within the xz-plane is not observed, that is seen, in particular, in Fig. 7. Namely, the long axis of the ellipse in the distribution $g_c(x,z)$ increases with increasing shear rate only in the shear direction [see Fig. 7(b)], whereas the small axis of the ellipse is practically unchanged both in the xy and xz-planes. This is a direct evidence that at high shear rates the nuclei are characterized by an elongated ellipsoidal shape. Note that this is in agreement with the results of [16,26,40,62].

The tilt angle φ between the gradient direction and the longest axis of the (ellipsoidlike) nucleus was determined directly from contours of the distribution $g_c(x,y)$. In Fig. 8,

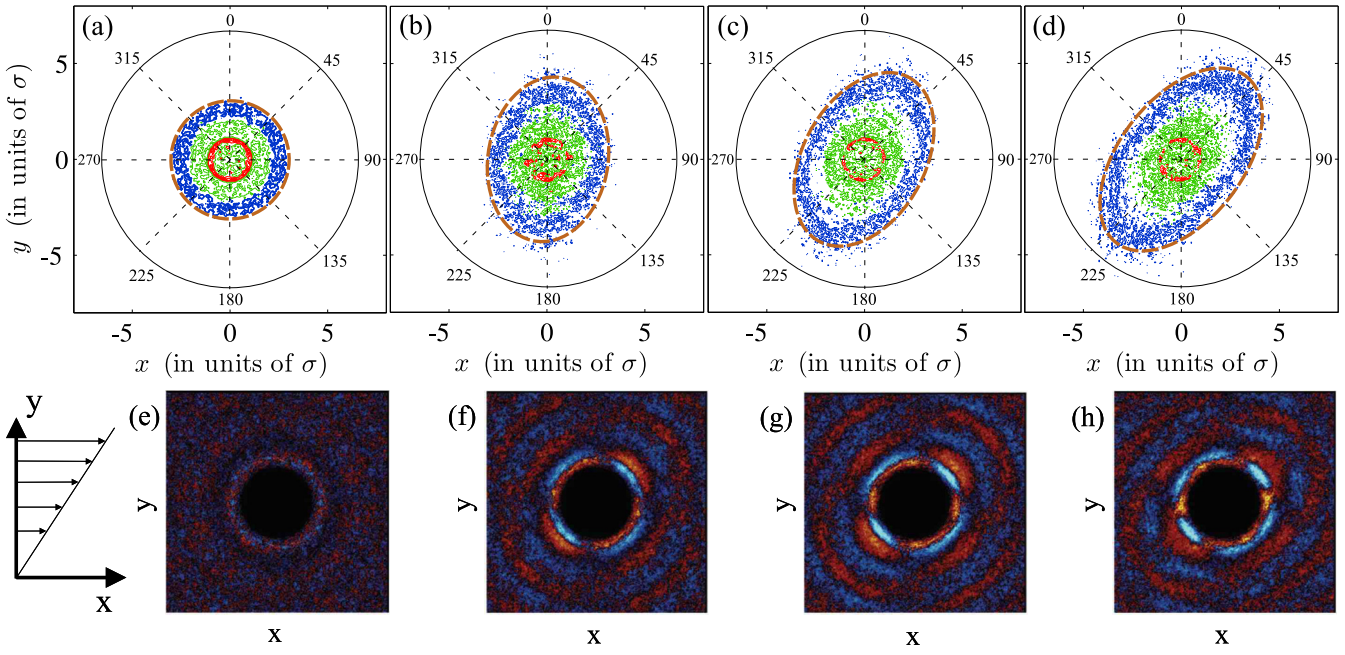

FIG. 6. Top: Projections of the pair distribution function $g_c(x,y)$ for the particles of a critically sized nucleus received for the system at the temperature $T = 0.15\,\epsilon/k_B$ and at the shear rates: (a) Zeroth shear rate, $\dot{\gamma} = 0$; (b) $\dot{\gamma} = 0.0005\,\tau^{-1}$ (critical deformation $\gamma_c \sim 3\%$); (c) $\dot{\gamma} = 0.005\,\tau^{-1}$ ($\gamma_c \sim 20\%$); (d) $\dot{\gamma} = 0.01\,\tau^{-1}$ ($\gamma_c \sim 50\%$). External boundaries of the distribution $g_c(x,y)$ are shown by the dashed circle and ellipses. Bottom: Projections of the pair distribution function onto shear-gradient xy-plane obtained for hard-sphere glassy systems at different shear strains: (e) 1%, (f) 10%, (g) 20%, and (h) 60% (taken from [21,32]).

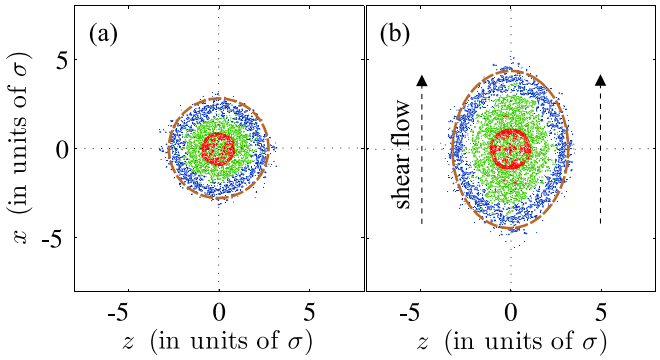

FIG. 7. Projections of the pair distribution function $g_c(x,z)$ onto the xz-planes for the particles of a critically sized nucleus received for the system at the temperature $T = 0.15\,\epsilon/k_B$ and at the shear rates: (a) $\dot{\gamma} = 0$; (b) $\dot{\gamma} = 0.01\,\tau^{-1}$. External boundaries of the distribution $g_c(x,z)$ are shown by the dashed circle and ellipse.

the γ_c-dependencies of φ obtained at different shear rates and temperatures are shown. The tilt angle φ increases with the increasing critical deformation γ_c according to the power-law dependence

$$\varphi(\gamma_c) = \varphi_0\{1 - \exp(-\mathcal{D}\gamma_c)\}. \tag{11}$$

Here, $\mathcal{D}$ and φ_0 are the positive fitting parameters. As it appears, both the parameters are independent on the temperature T for the considered temperature range and take the values $\mathcal{D} = 6.0\pm0.05$ and $\varphi_0 = 45^\circ\pm3^\circ$, respectively. The function $\varphi(\gamma_c)$ goes to saturation faster at the higher value of the parameter $\mathcal{D}$. The parameter φ_0 is the limit value of φ. Namely, at the large deformations (in our case at $\gamma_c > 0.6$) the long axis of the elliptic contour in the distribution $g_c(x,y)$ is oriented at the angle $\varphi_0 \approx 45^\circ$ with respect to the gradient direction (see also [11,20,32]). As it follows from [21,32], a pronounced anisotropy in the microscopic structure of hard-sphere suspensions and glasses is observed with increasing shear strain. It was found in [21,32] that with increasing shear deformation the particles density starts to be dependent on direction, and the so-called stretching and compression directions appear. It is remarkable that the contours of this distribution [see Fig. 6(e)–6(h)] are similar to the contours of the distribution $g_c(x,y)$ [see Fig. 6(a)–6(d)], where the angle between the stretching direction and the gradient direction goes to the limit value $\approx45^\circ$. On the other hand, it was experimentally found by Nosenko *et al.* [20] for the strongly coupled liquid that the microscopic structure of the system at influence of shear becomes anisotropic; and compressive and stretching axes tend to be oriented at the angle of $\pm45^\circ$ respective to the direction of flow. Evidently, such ellipticity of the distribution $g_c(x,y)$ arising at steady shear has an impact on the crystal nucleation processes and is also responsible for the critically sized nuclei asphericity.

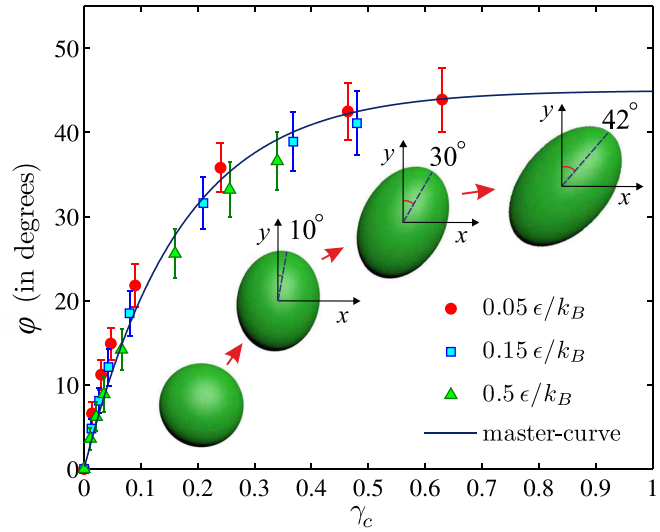

FIG. 8. Tilt angle φ of a critically sized nucleus as a function of the critical deformation γ_c at different temperatures. The solid curve is fit in Eq. (11). Insets: Schematic illustrations showing the change of orientation and shape of the nuclei at various γ_c.

C. Size and shape of critically sized nuclei

Let a_c and b_c be the small and large semiaxes of the elliptic contours in the distribution $g_c(x,y)$, respectively. The quantities a_c and b_c are evaluated from the distribution $g_c(x,y)$ at different critical deformation γ_c. As shown from Fig. 9, the small semiaxis a_c is practically unchanged with the increasing critical deformation γ_c, while the quantity b_c increases with γ_c. Remarkably, the γ_c-dependencies of the quantities are well reproduced by

$$a_c(\gamma_c) = a_0\{1 + \mathcal{A}\gamma_c^\kappa\} \tag{12}$$

and

$$b_c(\gamma_c) = a_0\{1 + \mathcal{B}\gamma_c^\kappa\}. \tag{13}$$

Here, a_0 is the radius of a spherical nucleus at $\dot{\gamma} = 0$, and it is $a_0 \simeq 2.71$, 2.81, and $2.87\,\sigma$ for temperatures $T = 0.05$, 0.15, and $0.5\,\epsilon/k_B$, respectively. The dimensionless parameters $\mathcal{A}$ and $\mathcal{B}$ take the fixed positive values $\mathcal{A} \simeq 0.004\pm0.001$ and $\mathcal{B} \simeq 0.42\pm0.04$ for the considered temperature range $T \in [0.05;\,0.5]\,\epsilon/k_B$. The dimensionless parameter κ is defined by the thermodynamic properties of a system and takes positive value $\kappa = 1/3$ for considered temperatures. We found that the ratio $\mathcal{B}/\mathcal{A}$ is ≈105 and,

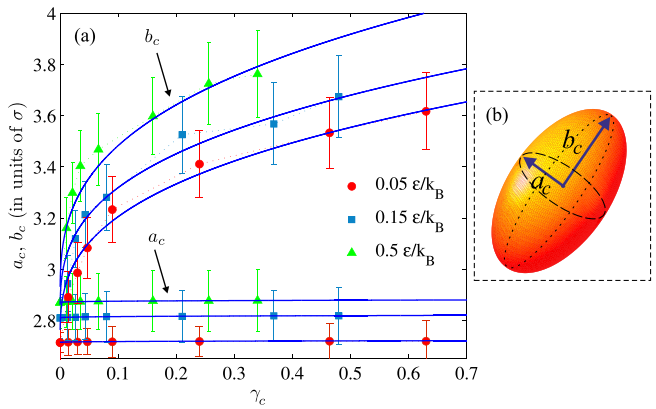

FIG. 9. (a) Quantities a_c and b_c as a function of the critical deformation γ_c. The solid curves are fit in Eqs. (12) and (13). (b) Schematic image of the ellipsoidal shape, where a_c and b_c are small and large semiaxes determined from the distribution $g_c(x,y)$.

consequently, the asphericity of a nucleus shape increases mainly due to the increase of the large semiaxis b_c.

From Eqs. (12) and (13), one obtains the γ_c-dependence of the critical size n_c

$$n_c(\gamma_c) = \frac{4}{3}\pi\rho_c[a_c(\gamma_c)]^2[b_c(\gamma_c)] = \frac{4}{3}\pi\rho_c a_0^2 b_0\{1 + \mathcal{B}\gamma_c^{\kappa} + 2\mathcal{A}\gamma_c^{\kappa} + 2\mathcal{A}\mathcal{B}\gamma_c^{2\kappa} + \mathcal{A}^2\gamma_c^{2\kappa} + \mathcal{A}^2\mathcal{B}\gamma_c^{2\kappa}\}. \quad (14)$$

Since the parameter $\mathcal{A}$ takes small values in the case of the Dz-system ($\mathcal{A} \simeq 0.004$) and taking into account $b_c \simeq a_c$ at $\dot{\gamma} = 0$, Eq. (14) can be rewritten in the following simplified form:

$$n_c(\gamma_c) = n_c(\dot{\gamma} = 0)\{1 + \mathcal{B}\gamma_c^{\kappa}\}, \quad (15)$$

where

$$n_c(\dot{\gamma} = 0) = \frac{4}{3}\pi\rho_c a_0^3. \quad (16)$$

Here, $\rho_c \simeq 1.04 \pm 0.02\,\sigma^{-3}$ is the numerical density of the crystalline phase. Figure 4(c) shows the fit of the simulation results in Eq. (15) at given values of $\mathcal{B}$, κ, and a_0. It can be seen from Fig. 4(c), Eq. (15) reproduces correctly the γ_c-dependence of the critical size n_c at the considered temperatures.

For the quantitative characterization of the nuclei shape, we define the deformation parameter

$$\chi = \frac{b_c - a_c}{b_c + a_c}. \quad (17)$$

For the case $b_c \geq a_c$, the parameter χ takes the values from the range $[0; 1]$. Namely, if a nucleus is characterized by a perfect spherical shape, we have $\chi = 0$, whereas for an elongated nucleus one has $\chi \to 1$.

The γ_c-dependencies of the parameter χ at different temperatures are shown in Fig. 10(a). An increase of χ with the critical deformation γ_c is mainly due to the increase of the value b_c. It should be noted that the γ_c-dependencies of S_0 and χ are correlated [see Figs. 4(c) and 10(a)]. Further, the results reveal that the γ_c-dependencies of the parameter χ are reproduced by

$$\chi(\gamma_c) = \frac{\mathcal{B}\gamma_c^{\kappa}}{2 + \mathcal{B}\gamma_c^{\kappa}}, \quad (18)$$

which follows from Eqs. (12), (13), and (17). Here, $\mathcal{B} \simeq 0.42 \pm 0.04$ and $\kappa \simeq 1/3$ for the considered temperatures. We found that the γ_c-dependencies of the parameter χ go to saturation at high critical deformations, and extremely high shear rates do not lead to the high asphericity of a nucleus.

Moreover, Fig. 10(b) shows the parameter χ as a function of the scaled critical size n_c/n_0. Here, the quantity n_0 is the critical size, which is evaluated for the system at absence of a shear, $n_0 \equiv n_c(\dot{\gamma} = 0)$. This figure presents our results as well as the results of flow-induced nucleation in polymer melts taken from [26,27]. Remarkably, all data collapse into a master-curve reproducible by

$$\chi(n_c) = \frac{n_c - n_0}{n_c + n_0}. \quad (19)$$

Equation (19) follows directly from Eqs. (15) and (18).

As shown from Fig. 10(b), values of n_c/n_0 and χ accessible to the considered Dz-system correspond to a narrower range in comparison with values for the polymer system. The Dzugutov interaction potential is not capable of forming elongated structures with large values of deformation

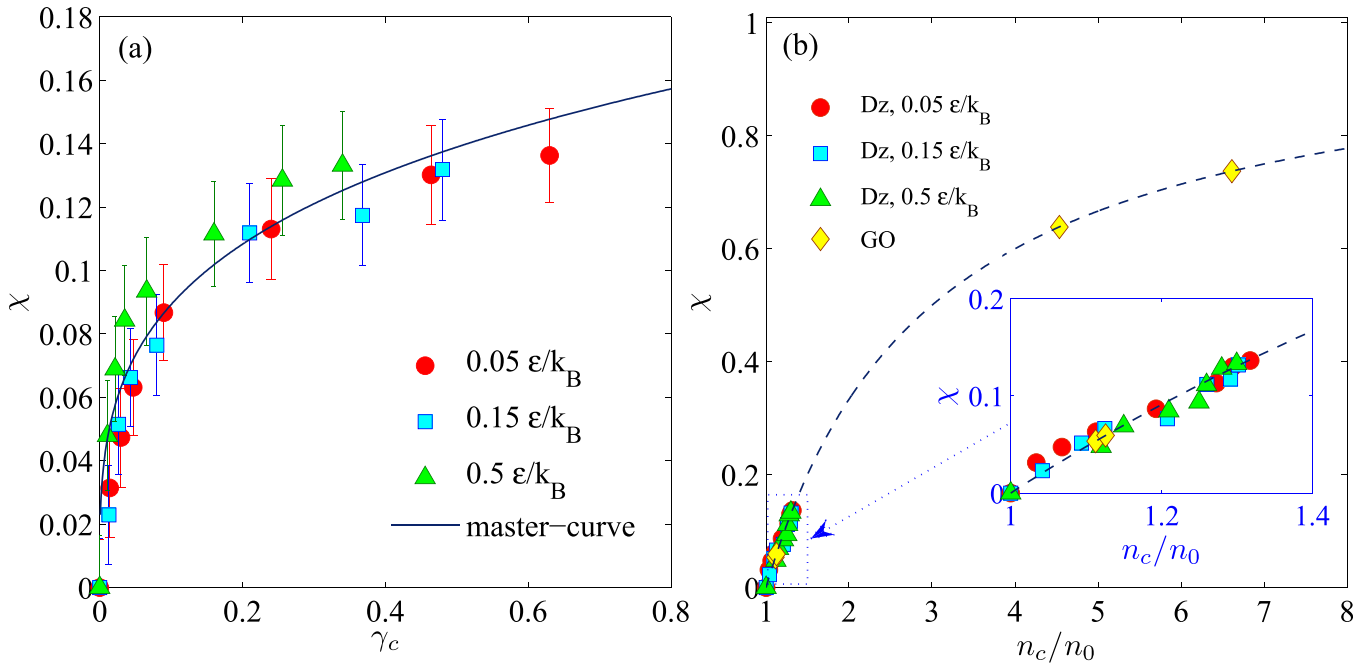

FIG. 10. (a) Quantity χ as a function of the critical deformation γ_c. The solid curve is fit in Eq. (18). (b) Quantity χ as a function of the scaled critical size n_c/n_0, where $n_0 \equiv n_c(\dot{\gamma} = 0)$ is the critical size at zeroth shear rate. The dashed curve is fit in Eq. (19). The data for elongated critically sized crystalline nuclei marked as *GO* are taken from [26,27].

parameter. Therefore, it is expected that the results for the Dzugutov pseudo-metallic system are located in the lower left part of the figure, whereas the data for the soft systems (say, polymers) have to be located at higher values of parameters. Results presented in Fig. 10(b) indicate on a possible universality in correlation between the characteristics of size and shape critically sized nucleus that does not depend on specific types of the considered systems. Therefore, additional studies of this point would be useful.

IV. CONCLUSION

The main results of this study are the following:

(i) The shear-induced structural ordering of the single-component glassy system is initiated through the crystal nucleation mechanism.

(ii) The critical size n_c and the nucleation time τ_c were evaluated at different fixed shear rates and temperatures. It is shown that both the size and the shape of the critically sized nuclei depend on the shear rate. The asphericity of the nuclei increases with the increasing shear rate $\dot{\gamma}$ (or with the increasing critical deformation $\gamma_c \equiv \dot{\gamma}\tau_c$); the larger asphericity of the nucleus corresponds to the larger critical size. It is verified by the increasing asphericity parameter S_0 and by the changes of the contours of $g_c(x, y)$ and $g_c(x, z)$ calculated for the particles of the critically sized nuclei.

(iii) The shapes of the critically sized nuclei change with increasing shear rate from spherical to ellipsoidal. The asphericity parameter and the critical size increase according to the power-law $\propto (\dot{\gamma}\tau_c)^{1/3}$.

(iv) It is shown that the ellipsoidal nuclei are oriented within the shear-gradient plane at moderate and high shear rates. The tilt angle of the nuclei increases with the increasing shear rate according to the power-law dependence.

(v) It is found that the scaled n_c-dependencies of the nuclei deformation parameter χ are collapsed into a unified master-curve.

ACKNOWLEDGMENTS

The work was supported in part by the grant MD-5792.2016.2 (program of support for young scientists in RF). Authors are grateful to the Ministry of Education and Science of the Russian Federation for supporting the research in the framework of the state assignment (No. 3.2166.2017/4.6). The molecular dynamic simulations were performed by using the computational clusters of Kazan Federal University and of Joint Supercomputer Center of RAS.

References

[1] Janeschitz-Kriegl, H., "Some remarks on flow induced crystallization in polymer melts," J. Rheol. **57**, 1057–1064 (2013).

[2] Scelsi, L., M. R. Mackley, H. Klein, P. D. Olmsted, R. S. Graham, O. G. Harlen, and T. C. B. McLeish, "Experimental observations and matching viscoelastic specific work predictions of flow-induced crystallization for molten polyethylene within two flow geometries," J. Rheol. **53**, 859–876 (2009).

[3] Berthier, L., and G. Biroli, "Theoretical perspective on the glass transition and amorphous materials," Rev. Mod. Phys. **83**, 587–645 (2011).

[4] Ediger, M. D., and P. Harrowell, "Perspective: Supercooled liquids and glasses," J. Chem. Phys. **137**, 080901 (2012).

[5] Greer, L. A., "Metallic glasses," Science **267**, 1947–1953 (1995).

[6] Lu, Z. P., and C. T. Liu, "Glass formation criterion for various glass-forming systems," Phys. Rev. Lett. **91**, 115505 (2003).

[7] Mokshin, A. V., and J.-L. Barrat, "Crystal nucleation and cluster-growth kinetics in a model glass under shear," Phys. Rev. E **82**, 021505 (2010).

[8] Löwen, H., "Colloidal soft matter under external control," J. Phys.: Condens. Matter **13**, R415–R432 (2001).

[9] Haw, M. D., W. C. K. Poon, and P. N. Pusey, "Colloidal glasses under shear strain," Phys. Rev. E **58**, 4673–4687 (1998).

[10] He, G.-L., R. Messina, H. Löwen, A. Kiriy, V. Bocharova, and M. Stamm, "Shear-induced stretching of adsorbed polymer chains," Soft Matter **5**, 3014–3017 (2009).

[11] Dasgupta, R., H. George, E. Hentschel, and I. Procaccia, "Microscopic mechanism of shear bands in amorphous solids," Phys. Rev. Lett. **109**, 255502 (2012).

[12] Evans, D. J., and G. P. Morriss, *Statistical Mechanics of Non-Equilibrium Liquids* (Cambridge University, New York, 2008).

[13] Fang, H., Y. Zhang, J. Bai, and Z. Wang, "Shear-induced nucleation and morphological evolution for bimodal long chain branched polylactide," Macromolecules **46**, 6555–6565 (2013).

[14] Butler, S., and P. Harrowell, "Kinetics of crystallization in a shearing colloidal suspension," Phys. Rev. E **52**, 6424–6430 (1995).

[15] Mokshin, A. V., B. N. Galimzyanov, and J.-L. Barrat, "Extension of classical nucleation theory for uniformly sheared systems," Phys. Rev. E **87**, 062307 (2013).

[16] Blaak, R., S. Auer, D. Frenkel, and H. Löwen, "Crystal nucleation of colloidal suspensions under shear," Phys. Rev. Lett. **93**, 068303 (2004).

[17] Kerrache, A., N. Mousseau, and L. J. Lewis, "Crystallization of amorphous silicon induced by mechanical shear deformations," Phys. Rev. B **84**, 014110 (2011).

[18] Shao, Z., J. P. Singer, Y. Liu, Z. Liu, H. Li, M. Gopinadhan, C. S. O'Hern, J. Schroers, and C. O. Osuji, "Shear-accelerated crystallization in a supercooled atomic liquid," Phys. Rev. E **91**, 020301 (2015).

[19] Mura, F., and A. Zaccone, "Effects of shear flow on phase nucleation and crystallization," Phys. Rev. E **93**, 042803 (2016).

[20] Nosenko, V., A. V. Ivlev, and G. E. Morfill, "Microstructure of a liquid two-dimensional dusty plasma under shear," Phys. Rev. Lett. **108**, 135005 (2012).

[21] Koumakis, N., M. Laurati, S. U. Egelhaaf, J. F. Brady, and G. Petekidis, "Yielding of hard-sphere glasses during start-up shear," Phys. Rev. Lett. **108**, 098303 (2012).

[22] Kumaraswamy, G., J. A. Kornfield, F. Yeh, and B. S. Hsiao, "Shear-enhanced crystallization in isotactic polypropylene. 3. Evidence for a kinetic pathway to nucleation," Macromolecules **35**, 1762–1769 (2002).

[23] Keller, A., and M. J. Machin, "Oriented crystallization in polymers," J. Macromol. Sci., Phys. B **1**, 41–91 (1967).

[24] Roozemond, P., and G. Peters, "Flow-enhanced nucleation of poly(1-butene): Model application to short-term and continuous shear and extensional flow," J. Rheol. **57**, 1633–1653 (2013).

[25] Roozemond, P., M. van Drongelen, Z. Ma, A. Spoelstra, D. Hermida-Merino, and G. Peters, "Self-regulation in flow-induced structure formation of isotactic polypropylene," Macromol. Rapid Commun. **36**, 385–390 (2015).

[26] Graham, R. S., and P. D. Olmsted, "Coarse-grained simulations of flow-induced nucleation in semicrystalline polymers," Phys. Rev. Lett. **103**, 115702 (2009).

[27] Graham, R., and P. Olmsted, "Kinetic Monte Carlo simulations of flow induced nucleation in polymer melts," Faraday Discuss. **144**, 71–92 (2010).

[28] McIlroya, C., and P. D. Olmsted, "Deformation of an amorphous polymer during the fused-filament-fabrication method for additive manufacturing," J. Rheol. **61**, 379–397 (2017).

[29] Viasnoff, V., and F. Lequeux, "Rejuvenation and overaging in a colloidal glass under shear," Phys. Rev. Lett. **89**, 065701 (2002).

[30] Rottler, J., and M. O. Robbins, "Shear yielding of amorphous glassy solids: Effect of temperature and strain rate," Phys. Rev. E **68**, 011507 (2003).

[31] Wallace, M. L., and B. Joós, "Shear-induced overaging in a polymer glass," Phys. Rev. Lett. **96**, 025501 (2006).

[32] Koumakis, N., M. Laurati, A. R. Jacob, K. J. Mutch, A. Abdellali, A. B. Schofield, S. U. Egelhaaf, J. F. Brady, and G. Petekidis, "Start-up shear of concentrated colloidal hard spheres: Stresses, dynamics, and structure," J. Rheol. **60**, 603–623 (2016).

[33] Koumakis, N., A. B. Schofieldc, and G. Petekidis, "Effects of shear induced crystallization on the rheology and ageing of hard sphere glasses," Soft Matter **4**, 2008–2018 (2008).

[34] Mokshin, A. V., and J.-L. Barrat, "Shear induced structural ordering of a model metallic glass," J. Chem. Phys. **130**, 034502 (2009).

[35] Shrivastav, G. P., P. Chaudhuri, and J. Horbach, "Heterogeneous dynamics during yielding of glasses: Effect of aging," J. Rheol. **60**, 835–847 (2016).

[36] Mokshin, A. V., and B. N. Galimzyanov, "Scaling law for crystal nucleation time in glasses," J. Chem. Phys. **142**, 104502 (2015).

[37] Kashchiev, D., *Nucleation: Basic Theory with Applications* (Butterworth-Heinemann, Oxford, 2000).

[38] Kelton, K. F., A. L. Greer, "The classical theory," Pergamon Mater. Ser. **15**, 19–54 (2010).

[39] Kalikmanov, V. I., *Nucleation Theory; Lecture Notes in Physics* (Springer, New York, 2012), Vol. 860.

[40] Wang, X. W., J. Ouyang, and Z. Liu, "A phase field technique for modeling and predicting flow induced crystallization morphology of semi-crystalline polymers," Polymers **8**, 230 (2016).

[41] Dzugutov, M., "Glass formation in a simple monatomic liquid with icosahedral inherent local order," Phys. Rev. A **46**, R2984–R2987 (1992).

[42] Roth, J., "Shock waves in materials with Dzugutov-potential interactions," Phys. Rev. B **72**, 014125 (2005).

[43] Mokshin, A. V., and J.-L. Barrat, "Shear-induced crystallization of an amorphous system," Phys. Rev. E **77**, 021505 (2008).

[44] Lees, Q. W., and S. F. Edwards, "The computer study of transport processes under extreme conditions," J. Phys. C: Solid State Phys. **5**, 1921–1929 (1972).

[45] Steinhardt, P. J., D. R. Nelson, and M. Ronchetti, "Bond-orientational order in liquids and glasses," Phys. Rev. B **28**, 784–805 (1983).

[46] Reinhardt, A., and J. P. K. Doye, "Free energy landscapes for homogeneous nucleation of ice for a monatomic water model," J. Chem. Phys. **136**, 054501 (2012).

[47] Mickel, W., S. C. Kapfer, G. E. Schröder-Turk, and K. Mecke, "Shortcomings of the bond orientational order parameters for the analysis of disordered particulate matter," J. Chem. Phys. **138**, 044501 (2013).

[48] ten Wolde, P. R., M. J. Ruiz-Montero, and D. Frenkel, "Numerical calculation of the rate of crystal nucleation in a Lennard-Jones system at moderate undercooling," J. Chem. Phys. **104**, 9932–9947 (1996).

[49] Mokshin, A. V., and B. N. Galimzyanov, "Steady-state homogeneous nucleation and growth of water droplets: Extended numerical treatment," J. Phys. Chem. B **116**, 11959–11967 (2012).

[50] Mokshin, A. V., and B. N. Galimzyanov, "Ordering in model metallic glass upon external homogeneous shear," Bull. Russ. Acad. Sci. Phys. **77**, 281–283 (2013).

[51] Roth, J., and A. R. Denton, "Solid-phase structures of the Dzugutov pair potential," Phys. Rev. E **61**, 6845–6857 (2000).

[52] Reguera, D., and J. M. Rubi, "Homogeneous nucleation in inhomogeneous media. II. Nucleation in a shear flow," J. Chem. Phys. **119**, 9888–9893 (2003).

[53] Lifshitz, E. M., and L. P. Pitaevskii, *Physical Kinetics* (Butterworth, Washington, 2006).

[54] Mokshin, A. V., and B. N. Galimzyanov, "Kinetics of the crystalline nuclei growth in glassy systems," Phys. Chem. Chem. Phys. **19**, 11340–11353 (2017).

[55] Weingartner, N. B., C. Pueblo, F. S. Nogueira, K. F. Kelton, and Z. Nussinov, "A phase space approach to supercooled liquids and a universal collapse of their viscosity," Front. Mater. **3**, 1–12 (2016).

[56] Holmqvist, P., M. P. Lettinga, J. Buitenhuis, and J. K. G. Dhont, "Crystallization kinetics of colloidal spheres under stationary shear flow," Langmuir **21**, 10976–10982 (2005).

[57] Tribout, C., B. Monasse, and J. M. Haudin, "Experimental study of shear-induced crystallization of an impact polypropylene copolymer," Colloid Polym. Sci. **274**, 197–208 (1996).

[58] Coccorullo, I., R. Pantani, and G. Titomanlio, "Spherulitic nucleation and growth rates in an iPP under continuous shear flow," Macromolecules **41**, 9214–9223 (2008).

[59] Zaccone, A., H. Wu, D. Gentili, and M. Morbidelli, "Theory of activated-rate processes under shear with application to shear-induced aggregation of colloids," Phys. Rev. E **80**, 051404 (2009).

[60] Shen, Y., S. B. Jester, T. Qi, and E. J. Reed, "Nanosecond homogeneous nucleation and crystal growth in shock-compressed SiO2," Nat. Mater. **15**, 60–65 (2016).

[61] Cugliandolo, L. F., J. Kurchan, and L. Peliti, "Energy flow, partial equilibration, and effective temperatures in systems with slow dynamics," Phys. Rev. E **55**, 3898–3914 (1997).

[62] Somani, R. H., L. Yang, B. S. Hsiao, T. Sun, N. V. Pogodina, and A. Lustiger, "Shear-induced molecular orientation and crystallization in isotactic polypropylene: Effects of the deformation rate and strain," Macromolecules **38**, 1244–1255 (2005).